JOURNAL OF MATERIALS SCIENCE 30 (1995) 4541–4548

The effect of interfacial imperfections on the micromechanical stress and strain distribution in fibre reinforced composites

P. A. KAKAVAS, N. K. ANIFANTIS, K. BAXEVANAKIS, D. E. KATSAREAS, G. C. PAPANICOLAOU*
Department of Mechanical Engineering, Composite Materials Group, University of Patras, Patras 26500, Greece

A mathematical model for the determination of micromechanical stress and strain distribution in a unidirectional fibre reinforced composite is developed. The model consists of three phases represented as concentric cylinders, including the existence of an interphase. Both fibre and matrix have well defined elastic properties, while the interphase properties follow an exponential law of variation. The effect of an abrupt variation of elastic properties at the fibre–interphase boundary on the micromechanical state of stress is also presented. The degree of adhesion between fibre and matrix is described by means of adhesion parameters introduced, and a parametric study is performed wherein the stress and strain distribution around the fibre are determined as a function of adhesion efficiency and fibre volume fraction. Analytical results were confirmed by means of a finite element technique introduced and applied to the model.

1 Introduction

High performance composites replace traditional materials in structural applications. This is largely due to the outstanding mechanical properties offerred by them when compared to metals on an equivalent weight basis. The adhesion between reinforcement and matrix plays an important role in the operation of composite material [1]. Fibre reinforced materials are characterized by anisotropy, heterogeneity and interfaces. These imperfections introduce complexities that mainly are due to interfacial phenomena. The interface appears to be a preferential diffusion sink for all impurities associated with the matrix, the fibre, the processing and the environment [2]. The interfacial region that exists between fibres and matrix is not infinitesimally small in thickness; there is a region of finite thickness where the composition changes from that of the bulk matrix to that of the reinforcement. Thus, the region is not strictly an interface, and is nowadays referred to as the "interphase" [3]. Based on the above mentioned variation of properties, one method for estimating fibre–matrix interaction is by determining the interphase composition profile [4]. It is through the interphase that stresses are transferred from the matrix to the fibre. Micromechanical stress distribution at the interface between fibre and matrix is known to influence the mechanical behaviour of composites. A large residual stress is believed to originate from the difference of thermal expansion coefficients between fibre and matrix. Also, stresses at the interface are expected to be different from the volume average stress. Thus, the interface is responsible for complex residual stress states which are not easily characterized [2].

Various mathematical models have been introduced either to predict the overall properties of a composite and/or to characterize their micromechanical behaviour in the interphase region. The effect of the conditions existing at the surface of the filler particles on the thermomechanical behaviour of a particulate composite was investigated in [5]. Under the assumption that the interphase is homogeneous and isotropic exhibiting perfect adhesion with both main phases, a theory was developed providing quantitative means of assessing the adhesion efficiency between the phases and its effect on the thermomechanical behaviour of the composite. Thermal expansion coefficient and volume fraction of the interphase of a large number of particulate composites were determined and the effect of various parameters were examined in [6]. The effect of the boundary interphase on the mechanism of thermomechanical load transfer across the interface in the case of composites reinforced with short fibres was theoretically investigated in [7]. The variation of the glass transition temperature with fibre direction of a highly filled unidirectional composite, consisting of an epoxy matrix reinforced with long glass fibres, was investigated experimentally and explained theoretically by means of the interphase concept in [8]. A model with inhomogeneous interphase and continuously

* To whom all correspondence should be addressed.

0022–2461

varying mechanical properties has been presented in [9]. The model was effective in evaluating the extent of the boundary interphase giving a quantitative criterion of the quality of adhesion. The variation of the thermal expansion coefficient in the region of the boundary interphase and its effect on the transverse and longitudinal thermal expansion coefficients in fibre reinforced composites was investigated in [10]. The variation of the thickness of the boundary interphase as a function of filler volume fraction in particulate composites was investigated in [11]. The influence of moisture absorption on the extent of the boundary interphase in particulate composites was thoroughly studied in [12]. A three-phase theoretical model taking into account different shapes of variation of the interphase modulus versus the polar radius between the fibre and the matrix of a unidirectional composite material was presented in [13], while the same basic idea was applied in particulate composites in [14]. The model was then extended for the prediction of the thermal expansion behaviour of particulates in [15]. The concept of the interphase was also successfully used to explain the elastic, viscoelastic and thermal behaviour of pretreated asbestos filled epoxy polymers in [16–19]. An abrupt variation of the elastic modulus at the fibre-interphase boundary was considered in the model presented in [20]. It was found that the discontinuity of the modulus considered at the interphase boundary does not affect the longitudinal modulus of elasticity of the model fibre composite. In contrast, it was stated that this discontinuity mainly affects the stress and strain fields developed around the fibre rather than overall modulus. Pagano and Tandon [21] have developed a model to approximate the elastic response of a composite body reinforced by coated fibres orientated in various directions. The fundamental representative volume element is a three-phase concentric circular cylinder under prescribed displacement components. The microstress distribution inside the fibre, the coating and the matrix has been determined under a uniform three-dimensional mechanical and/or hygrothermal loading. A parametric study has also been conducted to illustrate how a coating applied to the fibre influences the effective thermoplastic properties and can alter the state of stress at the fibre–matrix interface and thereby modify or control an observed mode of failure. The model can be used to provide material guidance for controlling the micromechanical failure modes. In the case of elastomeric materials, the existence of an interphase layer between the fibre and matrix, having an elastic modulus close to that of the elastomer in its glassy state was used in [22] in order to explain stress transfer mechanisms in single fibre composites. More recently, a mathematical model based upon the cell method was extended in order to describe three-phase composite materials containing an interpahse [23].

In the present work, a three-phase model has been developed in order to study the stress and strain fields developed in the region surrounding a fibre embedded in a matrix. An exponential law of variation for the elastic properties of the interphase material was considered. Adhesion parameters are also introduced in order to describe elastic discontinuities existed at the fibre–interphase boundary. Analytical results were verified by respective numerical ones derived from a specially developed finite element analysis.

2. Semi-analytical procedure

2.1. The proposed model

The most simple and accurate model for the analysis of fibre reinforced composites including an interphase is the representative volume element (RVE) [5–7, 14, 20]. For unidirectional fibre reinforced composites, this model consists of three phases, i.e. the fibre, the interphase and the matrix, with radii r_f, r_i and r_m respectively, as shown in the cross section, Fig. 1. In the following a short review of the geometric and elastic characteristics of the RVE is presented, for completeness.

The volume fraction for each phase is determined by the relationships

$$V_f = (r_f/r_m)^2 \tag{1a}$$

$$V_i = (r_i/r_m)^2 - V_f \tag{1b}$$

$$V_m = 1 - V_i - V_f \tag{1c}$$

where subscripts f, i and m denote fibre, interphase and matrix, respectively.

The radii of the fibre and matrix are well defined, while the interphase radius can be estimated by means of thermal capacity measurements [13]. The outer radius of the matrix, r_m, is not constant, but it depends on the volume fraction of the fibre, V_f. Indeed, from Equation (1a), it is easily shown that

$$r_m = r_f/(V_f)^{1/2} \tag{2}$$

By the same way, the thickness of the interphase is also dependent on the fibre volume fraction. Fig. 2 shows the variation of the non-dimensional extent of these phases as a function of fibre volume fraction.

The elastic properties of the interphase may be considered as variable, but they must fit to those of fibre and matrix at the boundary surfaces. Different laws of variation of these properties, namely linear, parabolic, hyperbolic and logarithmic have been considered in previous studies [13–15]. In all these cases

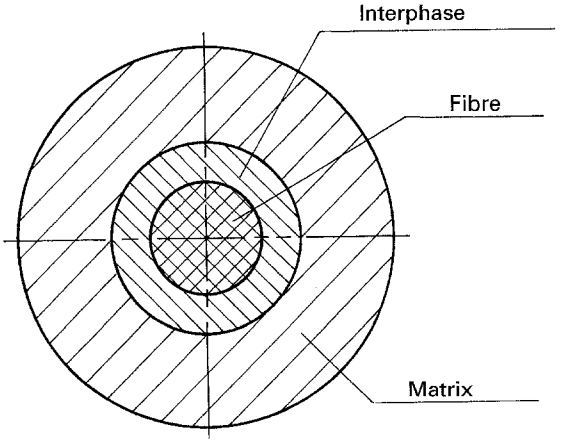

Figure 1 Cross-section of representative volume element.

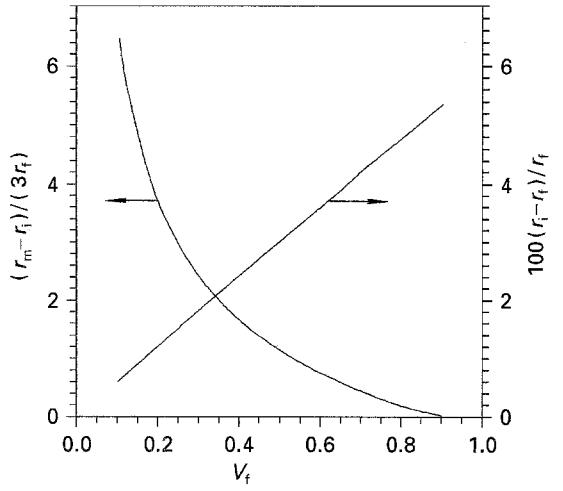

Figure 2 Variation of the reduced interphase thickness with fibre-volume fraction.

continuous variation at the interface between fibre and interphase was assumed. In real composite materials this is not true, depending on the interfacial conditions. Generally speaking, an abrupt variation at the fibre–matrix interface is expected. A proper way to introduce material inhomogeneities and imperfections is the use of proper adhesion parameters. The adhesion parameters α and β describe these conditions and are defined as follows:

$$\alpha = \frac{E_{i(r=r_f)}}{E_f} \tag{3a}$$

$$\beta = \frac{\nu_{i(r=r_f)}}{\nu_f} \tag{3b}$$

where E is the modulus of elasticity. For $\alpha = \beta = 1$, a continuous variation of the elastic properties is obtained at $r = r_f$. For $\alpha = E_m/E_f$ and $\beta = \nu_m/\nu_f$ a two-phase model is obtained consisting of fibre and matrix only. Whereas adhesion parameters are defined as ratios of individual elastic properties, due to their spatial variation, they depend on each other. A functional relationship between them of the following form may be assumed

$$\alpha = \frac{\kappa}{\beta} + \lambda \tag{4}$$

The constants κ and λ may be computed from the compatibility conditions imposed on α and β at $r = r_f$

$$\text{for } \alpha = 1 \Rightarrow \beta = 1$$

$$\text{for } \alpha = E_m/E_f \Rightarrow \beta = \nu_m/\nu_f \tag{5}$$

It follows that

$$\kappa = \frac{1 - \bar{E}}{1 - \bar{\nu}} \tag{6a}$$

$$\lambda = \frac{\bar{E} - \bar{\nu}}{1 - \bar{\nu}} \tag{6b}$$

where $\bar{E} = E_m/E_f$ and $\bar{\nu} = \nu_f/\nu_m$

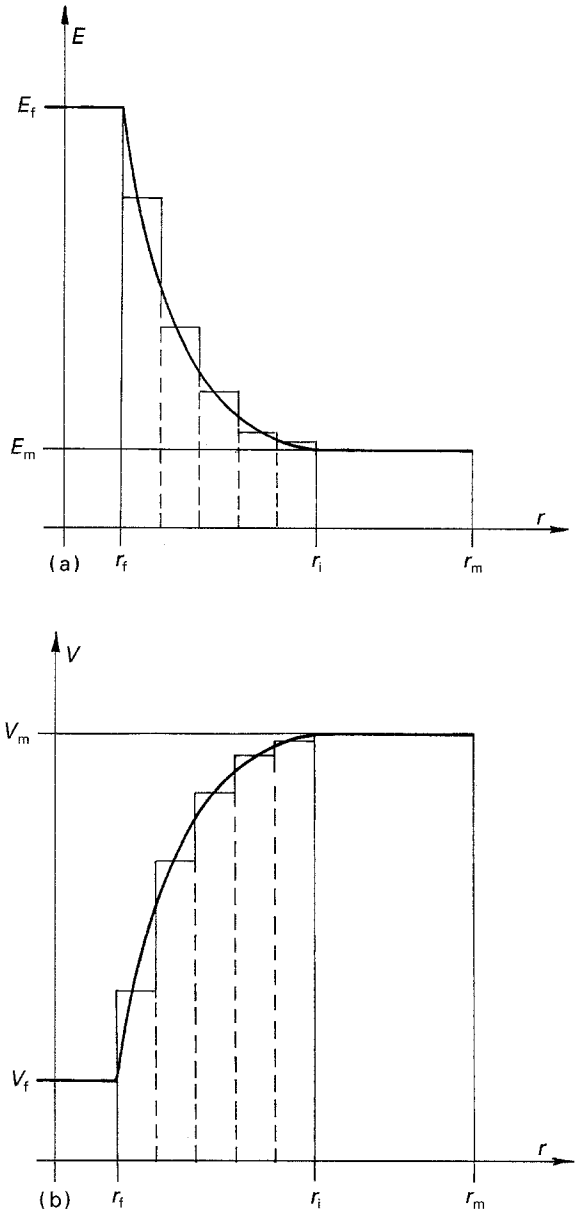

Figure 3 Variation of the elastic properties within the interphase: (a) modulus of elasticity, and (b) Poisson's ratio.

In the subsequent analysis it is assumed that interphase material inhomogeneity is described by an exponential law as follows (Fig. 3) :

$$E_i(r) = Ar\exp^{-Cr} + B \tag{7a}$$

$$\nu_i(r) = A'r\exp^{C'r} + B' \tag{7b}$$

The constants A, B, C, A′, B′ and C′ will be determined by the boundary conditions of the problem. The compatibility and continuity conditions at the boundary interfaces between various phases have as follows

$$E_{i(r=r_f)} = \alpha E_f, \qquad \nu_{i(r=r_f)} = \beta\nu_f \tag{8a}$$

$$E_{i(r=r_m)} = E_m, \qquad \nu_{i(r=r_m)} = \nu_m \tag{8b}$$

$$\left.\frac{dE_i}{dr}\right|_{r=r_m} = \left.\frac{d\nu_i}{dr}\right|_{r=r_m} = 0 \tag{8c}$$

From Equation 8a it is evident that the slope discontinuity is governed by adhesion parameters. Substitution of Equation 8a–c into Equation 7a–b leads to the following expressions for the variation of the modulus

of elasticity and the Poisson's ratio, respectively, within the interphase

$$E_i(\bar{r}) = E_m + (\alpha E_f - E_m)R(\bar{r}) \quad (9a)$$

$$\nu_i(\bar{r}) = \nu_m + (\beta \nu_f - \nu_m)R(\bar{r}) \quad (9b)$$

Spatial parameters appearing in Equation 9 are defined as follows

$$R(\bar{r}) = \frac{1 - \bar{r}\exp^{1-\bar{r}}}{1 - \bar{r}_f \exp^{1-r_f}} \quad (10)$$

where

$$\bar{r} = \frac{r}{r_i} \quad (11a)$$

$$\bar{r}_f = \frac{r_f}{r_i} = [V_f/(V_i + V_f)]^{1/2} \quad (11b)$$

From Equation 9 it is clear that interphase material inhomogeneity depends on the adhesion efficiency between fibre and matrix, as well as on the volume fraction of constituents. Thus, the model developed depends directly on the above parameters.

2.2. Analytical determination of stress and strain fields

The representative volume element as previously defined may be used for the elastic analysis of unidirectional fibre reinforced composites. To solve the unidirectional problem, the equivalent one of an internally pressurized cylinder of inner and outer radii, r_f and r_m, respectively, is analysed. In the following stress analysis, a plane stress problem was assumed. The components of strain in cylindrical co-ordinates under plane stress conditions are given by

$$\varepsilon_{rr} = \frac{1}{E}(\sigma_{rr} - \nu\sigma_{\vartheta\vartheta}) \quad (12a)$$

$$\varepsilon_{\vartheta\vartheta} = \frac{1}{E}(\sigma_{\vartheta\vartheta} - \nu\sigma_{rr}) \quad (12b)$$

$$\varepsilon_{zz} = \frac{1}{E}[-\nu(\sigma_{rr} + \sigma_{\vartheta\vartheta})] \quad (12c)$$

where σ_{rr}, $\sigma_{\theta\theta}$, ε_{rr}, $\varepsilon_{\theta\theta}$ and ε_{zz} denote radial, hoop and axial stresses and strains respectively. Similarly, the stress field is defined by

$$\sigma_{rr} = \frac{1}{r}\frac{d\Phi(r)}{dr} \quad (13a)$$

$$\sigma_{\vartheta\vartheta} = \frac{d^2\Phi(r)}{dr^2} \quad (13b)$$

$$\sigma_{r\vartheta} = 0 \quad (13c)$$

where $\Phi(r)$ is Airy's stress function. The appropriate Airy's stress function that satisfies the given stress field is

$$\Phi(r) = C\ln(r/K) + Br^2 \quad (14)$$

where C, K and B are constants, to be determined from the imposed boundary conditions of the problem. Applying Equation (13) in each phase of the RVE one finds, [13]

$$\sigma_{rr_{(r=r_f)}} = \sigma_{\vartheta\vartheta_{(r=r_f)}} = 2B_f \quad (15a)$$

$$\sigma_{rr_{(r=r_m)}} = \frac{C_m}{r^2} + 2B_m \quad (15b)$$

$$\sigma_{\vartheta\vartheta_{(r=r_m)}} = -\frac{C_m}{r^2} + 2B_m \quad (15c)$$

$$\sigma_{rr_{(r_f \leqslant r \leqslant r_i)}} = \frac{C_i}{r^2} + 2B_i \quad (15d)$$

$$\sigma_{\vartheta\vartheta_{(r_f \leqslant r \leqslant r_i)}} = -\frac{C_i}{r^2} + 2B_i \quad (15e)$$

where B_f, C_f, B_m ..., are constants to be determined. Substitution of Equation 15d and e into Equation 12 gives the following strain components

$$\varepsilon_{rr_{(r_f \leqslant r \leqslant r_i)}} = \frac{C_i}{2G_i r^2} + \frac{(1-\nu_i)}{G_i(1+\nu_i)}B_i \quad (16a)$$

$$\varepsilon_{\vartheta\vartheta_{(r_f \leqslant r \leqslant r_i)}} = -\frac{C_i}{2G_i r^2} + \frac{(1-\nu_i)}{G_i(1+\nu_i)}B_i \quad (16b)$$

Integration of Equation 16a within the interphase gives the radial displacement, i.e.

$$u_{rr_{(r_f \leqslant r \leqslant r_i)}} = -\frac{C_i}{2G_i r} + \frac{(1-\nu_i)}{G_i(1+\nu_i)}B_i r \quad (17)$$

where G_i denotes the shear modulus in the interphase, and it is equal to

$$G_i = \frac{E_i}{2(1+\nu_i)} \quad (18)$$

The boundary conditions for the radial stress at $r = r_f$ and $r = r_m$ are

$$\sigma_{rr_{(r=r_f)}} = -p_0 \quad (19a)$$

$$\sigma_{rr_{(r=r_m)}} = 0 \quad (19b)$$

where p_0 denotes the pressure applied on the inner surface of the interphase. In order to account for the variable elastic properties of the interphase it is assumed that it consists of N coaxial ring type elements, as shown in Fig. 4. Within each jth ring element it is assumed that the elastic properties E_i^j and ν_i^j remain constant. However, an exponential law of variation of the elastic properties is assumed to hold between adjacent elements, as is shown in Fig. 4. For two adjacent ring elements, j and $j+1$, the following compatibility and

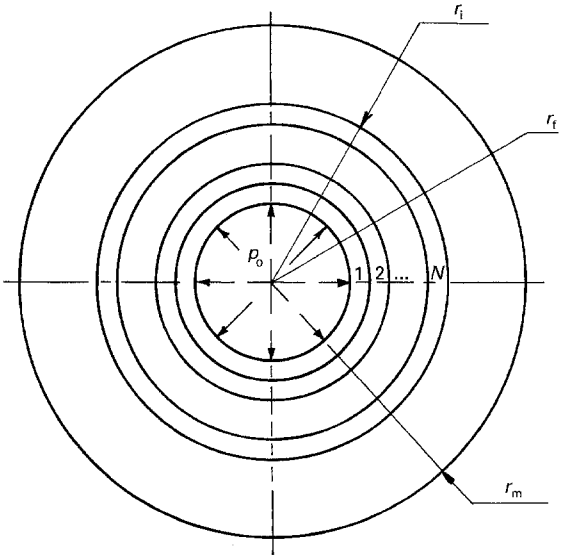

Figure 4 Discretization of interphase in N coaxial rings.

continuity conditions exist at their common boundaries, i.e.

$$u_{rr}^{j} = u_{rr}^{j+1} \tag{20a}$$

$$\sigma_{rr}^{j} = \sigma_{rr}^{j+1}, \quad j = 2, 3, \ldots, N+1 \tag{20b}$$

Applying Equation 20 successively at $r = r_1 = r_f$, $r = r_2, \ldots, r = r_{N+2} = r_m$ and substituting into Equations 15d and 17, respectively, the coefficients B_i and C_i may be determined. For example at $r = r_j$

$$\frac{C_{j-1}}{r_j^2} + 2B_{j-1} = \frac{C_j}{r_j^2} + 2B_j \tag{21a}$$

$$\frac{-C_{j-1}}{2G_{j-1}r_j} + \frac{1-\nu_{j-1}}{1+\nu_{j-1}}\frac{r_j}{G_{j-1}}B_{j-1} = \frac{-C_j}{2G_j r_j} + \frac{1-\nu_j}{1+\nu_j}\frac{r_j}{G_j}B_j \tag{21b}$$

$$j = 2, 3, \ldots, N+1$$

When $j = 1$

$$\frac{C_1}{r_1^2} + 2B_1 = -p_0 \tag{21c}$$

For $j = N + 2$

$$\frac{C_{N+1}}{r_{N+2}^2} + 2B_{N+1} = 0 \tag{21d}$$

Rearranging Equation 21 and properly assembling it, it follows that

$$[M]\boldsymbol{c} = \boldsymbol{P} \tag{22}$$

where

$$[M] = \begin{bmatrix} \frac{1}{r_1^2} & 2 & 0 & 0 & . & 0 & 0 & 0 & 0 \\ \frac{1}{r_2^2} & 2 & -\frac{1}{r_1^2} & -2 & . & 0 & 0 & 0 & 0 \\ \frac{-1}{2G_1 r_2} & \lambda_1\frac{r_2}{G_1} & \frac{1}{2G_2 r_2} & -\lambda_2\frac{r_2}{G_2} & . & 0 & 0 & 0 & 0 \\ . & . & . & . & . & . & . & . & . \\ 0 & 0 & 0 & 0 & . & \frac{1}{r_{N+1}^2} & 2 & \frac{-1}{r_{N+1}^2} & -2 \\ 0 & 0 & 0 & 0 & . & \frac{-1}{2G_N r_{N+1}} & \lambda_N\frac{r_{N+1}}{G_N} & \frac{1}{2G_{N+!}r_{N+1}} & -\lambda_{N+1}\frac{r_{N+1}}{G_{N+1}} \\ 0 & 0 & 0 & 0 & . & 0 & 0 & \frac{1}{r_{N+2}^2} & 2 \end{bmatrix} \tag{23a}$$

$$\boldsymbol{c} = \{C_i^1 B_i^1 C_i^2 B_i^2 \ldots C_i^{N+1} B_i^{N+1}\}^T \tag{23b}$$

$$\boldsymbol{P} = \{-p_0 0 0 \ldots 0\}^T \tag{23c}$$

with

$$\lambda_j = \frac{1-\nu_j}{1+\nu_j}, \quad j = 1, 2, \ldots, N+1 \tag{24}$$

where λ denotes the transpose vector. The dimension of the square matrix defined in Equation 23a is $2(N+2)-2$, where N denotes the number of rings within the interphase. Equation 22 describes the imposed boundary value problem in a step wise manner. A numerical solution of this equation provides all unknown constants which are needed for the elastic solution to be evaluated. As the number, N, of ring type elements increases, this solution approaches the exact solution of the problem.

2.3. Finite element approach

The elastic RVE problem stated in previous sections was solved using the finite element technique for reasons of comparison of the accuracy of the ring type element approach already presented. Plane stress conditions were assumed considering a very long fibre compared to its diameter. Due to the axisymmetric nature of the problem only a small slice of the cross-section was considered in the analysis. Fig. 5 depicts the domain of the RVE which was discretized in finite elements along the numerical solution of the problem under consideration. The angle of this sector was taken small enough in order to obtain an acceptable ratio for the elements' dimensions. The domain was discretized in 180 quadratic elements [24–26], from which half of them were located in interphase and the rest in the matrix. The total number of nodal points was 690. The 90 elements within the interphase correspond to 30 ring type elements, as in the case of the analytical approach of the problem. Also, the boundary conditions were the same, as in the analytical approach.

The material properties of the fibre and matrix remain constant. Instead, the elastic properties within

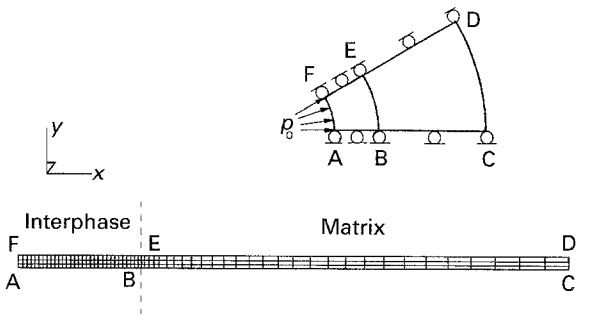

Figure 5 Finite element discretization.

the interphase vary exponentially according to Equation 9, but remain constant over each element as they are evaluated as averaged values. These values were introduced in the finite element algorithm, so that the variable elastic properties within the interphase were taken into account. The uniform internal pressure, p_0, was applied to the internal edge of each finite element at the fibre–interphase boundary. A constant value of $p_0 = 1$ MPa was assigned for the internal pressure.

The discretized form of equilibrium, compatibility and continuity equations leads to the following linear system of equations [26]

$$[K]\boldsymbol{u} = \boldsymbol{f} \tag{25}$$

where $[K]$ denotes the stiffness matrix whose coefficients are functions of the geometry and elastic properties; $\boldsymbol{u}$ indicates the vector of nodal displacements and $\boldsymbol{f}$ is the vector of the applied external forces. Numerical solution of Equation 25 leads to the evaluation of nodal displacements and averaged stresses and strains.

3. Results

In the following some numerical results are given to illustrate the proposed method and to confirm its accuracy. Material properties used in this study correspond to glass fibre composite (permaglass XE5/1, Permali Ltd, UK) consisting of an epoxy matrix reinforced with long E-glass fibres. The matrix material was based on a diglycidyl amine hardener (araldite MY 750/HT972, Ciba-Geigy, UK). The glass fibres had a radius of $r_f = 6$ μm and V_f varied from 0.4 to 0.7. The modulus of elasticity and Poisson's ratio for the fibre and matrix were: $E_f = 69.9$ GPa, $\nu_f = 0.2$, $E_m = 3.2$ GPa and $\nu_m = 0.2$ [20]. A computer algorithm was developed in order to evaluate the adhesion parameters α and β for different values of volume fraction, V_f, of the fibre. Within each ring element the elastic constants E_i and ν_i were computed using Equation 9, and the coefficients of the matrix $[M]$ were computed using the averaged values of elastic properties in each ring element within the interphase. The pressure, P_0, was taken as minus one, in order to normalize the stress and strain fields. The interphase was discretized into 30 coaxial ring elements of equal thickness and the matrix in five rings.

Results derived from both the finite element solution and the analytical model for the normalized stresses and strains are shown in Fig. 6a, b for comparison. Results shown in these figures refer to some specific values of the involved parameters, V_f, r_f, r_i and r_m, while two extreme values of the adhesion parameter, α, were considered. A strong effect of the adhesion parameter, α, on the stress and strain fields developed around the fibre is always present. Especially in the area of the interphase, an abrupt variation of the absolute values of both the radial and hoop stresses (Fig. 6a), as well as of the radial and hoop strains (Fig. 6b), takes place. Therefore, the interphase area has to be considered as a critical zone. In all cases, an excellent agreement between the two approaches is

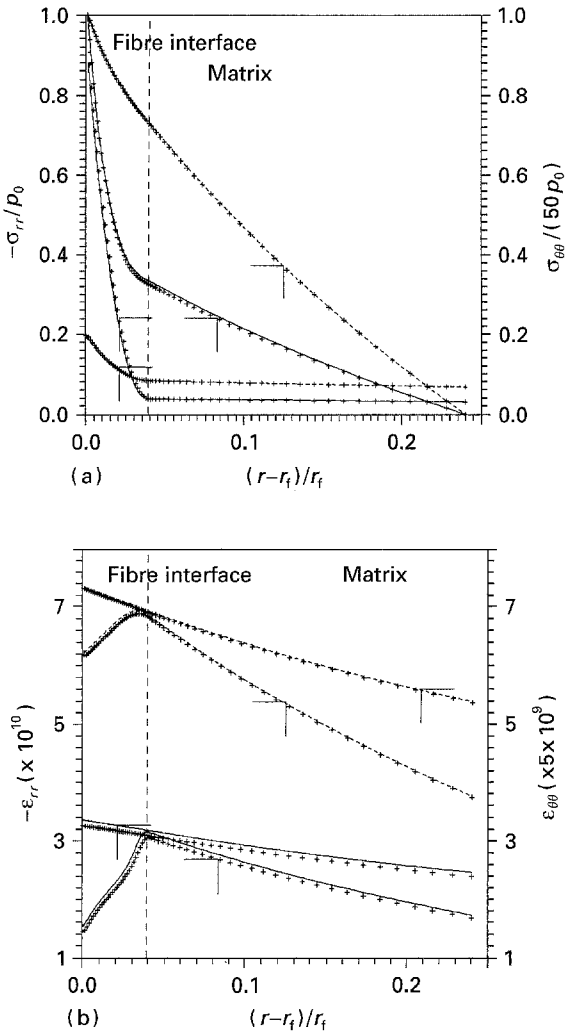

Figure 6 Comparison between analytical [(—) $\alpha = 1.0$ and (----) $\alpha = 0.1$] and (+ + +) finite element approaches (FEA) at $V_f = 0.65$, $r_f = 6$ μm, $r_i = 6.235$ μm and $r_m = 7.442$ μm: (a) normalized stresses, and (b) strains.

observed. Finally, as observed, there was no significant increase in the sensitivity of the finite element solution when a more dense finite element mesh was applied.

Fig. 7a, b depicts the normalized radial and hoop stress distributions, respectively, within the composite material, as a function of non-dimensional radial position, for various values of fibre volume fraction and adhesion parameter, α. Results for four different values of V_f and two different values of α are shown. In all cases, a high rate of stress variation was found to exist within the interphase area. Moreover, as the adhesion coefficient decreases, lower radial stresses are developed within the composite material. Also, the higher the volume fraction, the higher the radial stress developed at the same radial position. Fig. 7b shows that for a given radial distance, the normalized hoop stress increases with increasing fibre-volume fraction. Contrary, the normalized hoop stress was found to decrease as the adhesion parameter decreased.

Fig. 8a shows the radial strain distribution for four different values of the fibre-volume fraction and two extreme values of the adhesion parameter. From this figure it becomes clear, that the radial strain increases as the volume fraction increases, while for the same

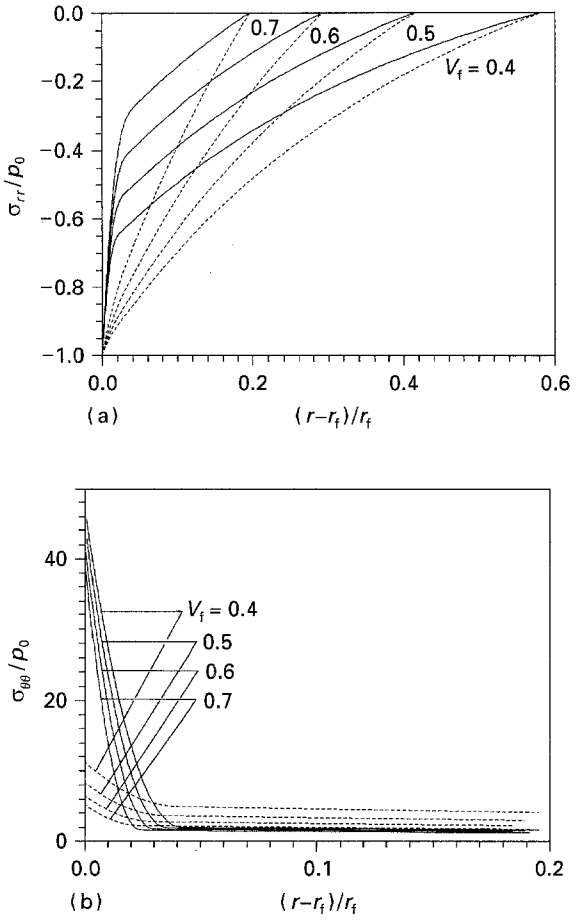

Figure 7 Distribution of normalized stresses at (—) $\alpha = 1.0$ and (- - -) $\alpha = 0.1$: (a) radial stress, and (b) hoop stress.

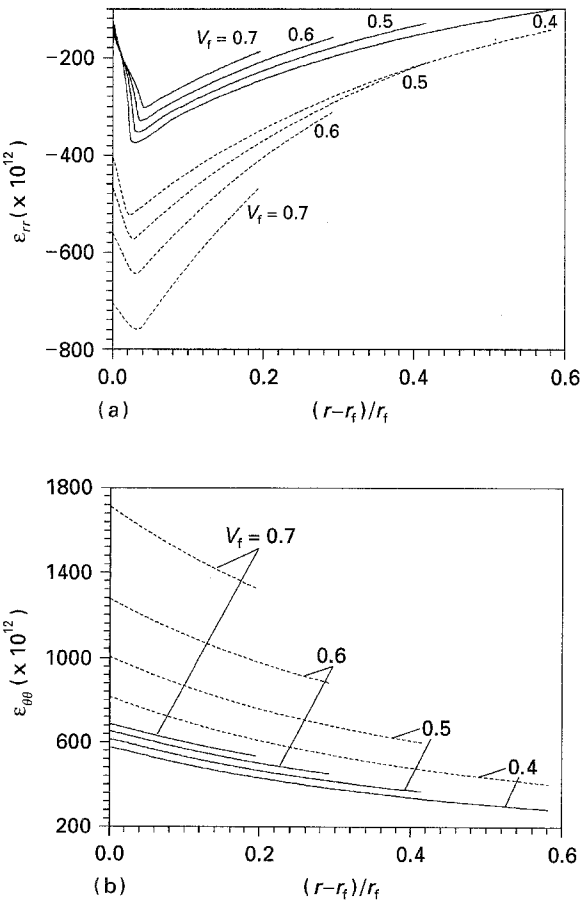

Figure 8 Distribution of strains at (—) $\alpha = 1.0$ and (- - -) $\alpha = 0.1$: (a) radial strain, and (b) tangential strain.

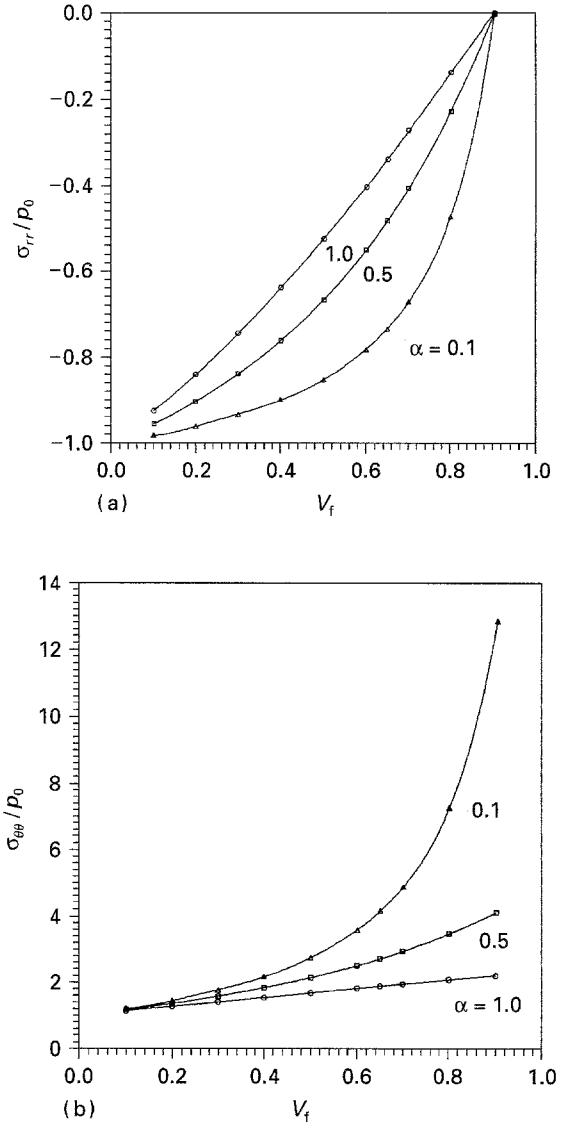

Figure 9 Variation of (a) radial and (b) tangential stresses at $r = r_i$ versus fibre volume fraction where $E_f/E_m = 21.844$.

volume fraction and fixed position, the radial strain decreases as the adhesion parameter decreases. Once again, the highest rate of variation of the radial strain is observed within the interphase material. In all cases, the radial strain passes a minimum which always lies at the matrix–interphase boundary, $r = r_i$. It is recalled that the interphase radius, r_i, depends on the fibre-volume fraction and it is independent of the parameter α.

Fig. 8b depicts the tangential strain distribution within the composite material. One observes that for a fixed value of adhesion parameter and radial distance, $\varepsilon_{\theta\theta}$ increases as the fibre-volume fraction increases. Also the $\varepsilon_{\theta\theta}$ component increases as the parameter α attains higher values. Contrary to the ε_{rr} distribution which shows a minimum at $r = r_i$, $\varepsilon_{\theta\theta}$ distribution does not exhibit a minimum value at this position, but uniformly decreases from the interphase to the matrix material.

The variation of the normalized radial and hoop stresses at the radial position $r = r_i$, as a function of the fibre-volume fraction and for three different values of the adhesion parameter is shown in Fig. 9a, b, respectively. In all cases, an increase of the stresses with

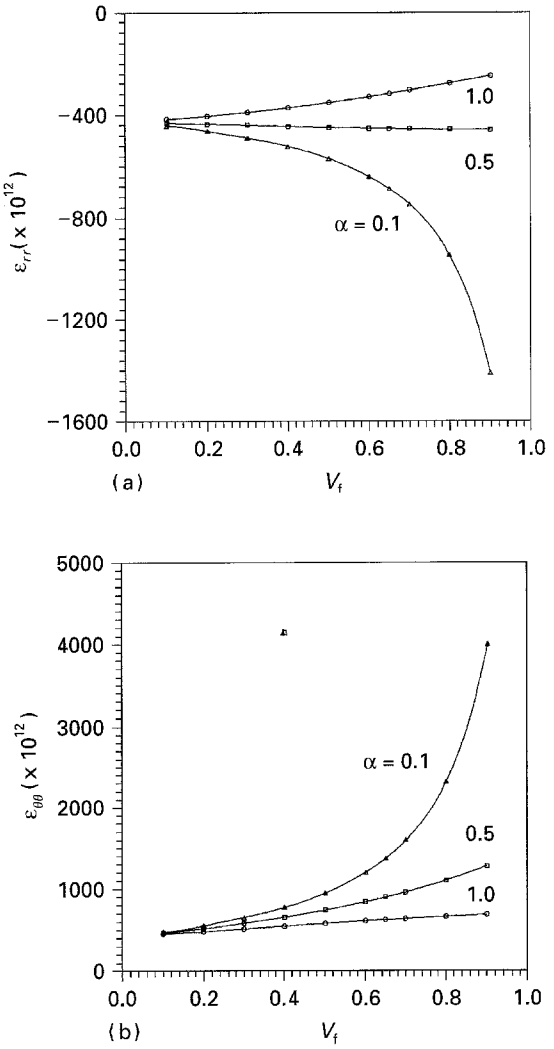

Figure 10 Variation of (a) radial and (b) tangential strains at $r = r_i$ versus fibre volume fraction where $E_f/E_m = 21.844$.

increasing fibre-volume fraction and adhesion coefficient is observed. The opposite type of variation has been observed when the effect of fibre-volume fraction and adhesion coefficient on the strain field developed around the fibres was studied (Fig. 10a, b).

4. Conclusions

An analytical model has been proposed for the computation of stress and strain distributions in unidirectional fibre reinforced composites. It was found that the radial stress decreases as adhesion between fibre and matrix is poor. The radial stress reduces also, as the fibre volume fraction decreases. The same behaviour is observed for the hoop stresses. The radial strain always passes through a minimum value. Instead, the hoop strain reduces smoothly. The analytical approach developed in this work was compared with a finite element approach. An excellent agreement between the results derived by the two methods was achieved. The proposed method may be extended and used for the failure analysis of fibre reinforced composites.

References

1. S. M. VRATSANOS, E. L. THOMAS and R. J. FARRIS, in "Proceedings of the First International Conference on Composite Interfaces (ICCI-I)", edited by Hatsuo Ishida and J. L. Koening (North-Holland, Cleveland, OH, 1986) pp. 151–160.
2. L. D. BROWN, B. MARUYAMA, Y. M. CHEONG, L. K. RABENBERG and H. L. MARCUS, in *ibid.* pp. 27–35.
3. M. R. PIGGOTT, A. SANADI, P. S. CHUA and D. ANDISON, in *ibid.* pp. 109–121.
4. R. EVERETT, W. HENSHAW, D. G. SIMONS and D. J. LANDS, in *ibid.* pp. 231–240.
5. G. C. PAPANICOLAOU, S. A. PAIPETIS and P. S. THEOCARIS, *Colloid and Polym. Sci.* **256** (1978) 625.
6. G. C. PAPANICOLAOU and P. S. THEOCARIS, *ibid.* **257** (1979) 239.
7. P. S. THEOCARIS and G. C. PAPANICOLAOU, *Fibre Sci. Technol.* **12**(6) (1979) 421.
8. *Idem, Colloid Polym. Sci.* **258** (1980) 1044.
9. G. C. PAPANICOLAOU, P. S. THEOCARIS and G. D. SPATHIS, *ibid.* **258** (1980) 1231.
10. P. S. THEOCARIS, G. C. PAPANICOLAOU and G. D. SPATHIS, *Fibre Sci. Technol.* **15** (1981) 187.
11. P. S. THEOCARIS, G. C. PAPANICOLAOU and E. P. SIDERIDIS, *J. Reinforced Plastics & Compos.* **1** (1982) 92.
12. P. S. THEOCARIS, G. C. PAPANICOLAOU and E. A. KONTOU, *J. Appl. Polym. Sci.* **28** (1983) 3145.
13. P. S. THEOCARIS, E. P. SIDERIDIS and G. C. PAPANICOLAOU, *J. Reinforced Plastics Compos.* **4** (1985) 396.
14. E. P. SIDERIDIS, P. S. THEOCARIS and G. C. PAPANICOLAOU, *Rheologica Acta* **25** (1986) 350.
15. E. P. SIDERIDIS and G. P. PAPANICOLAOU, *ibid.* **25** (1986) 350.
16. C. D. PAPASPYRIDES, T. DUVIS and G. C. PAPANICOLAOU, *Mater. Chem. Phys.* **17** (1987) 531.
17. G. C. PAPANICOLAOU and C. D. PAPASPYRIDES, *ibid.* **17** (1987) 453.
18. C. D. PAPASPYRIDES and G. C. PAPANICOLAOU, *J. Appl. Polym. Sci.* **36** (1988) 309.
19. G. C. PAPANICOLAOU and C. D. PAPASPYRIDES, *Compos. Sci. Technol.* **31** (1988) 261.
20. G. C. PAPANICOLAOU, G. J. MESSINIS and S. S. KARAKATSANIDIS, *J. Mater. Sci.* **24** (1989) 395.
21. N. J. PAGANO and G. P. TANDON, *Compos. Sci. Technol.* **31** (1988) 273.
22. E. M. ASLOUM, M. NARDIN and J. SCHULTZ, *J. Mater. Sci.* **24** (1989) 1835.
23. S. D. GARDNER, C. U. PITTMAN Jr and R. M. HACKETT, *Compos. Sci. Technol.* **46** (1993) 307.
24. K. J. BATHE, "Finite Element Procedures in Engineering Analysis" (Englewood Cliffs, N J, 1982).
25. J. T. ODEN, "Finite Elements of Non-linear Continua" (McGraw-Hill, New York, 1972).
26. FEA, "Finite Element System, User Manual", Version 11, Forge House, 66 High Street Kingston-Upon-Thames, Surrey, KT1 1HN (1993).

Received 10 August 1994
and accepted 22 March 1995